Article

Tropical Cyclone Wind Field Reconstruction and Validation Using Measurements from SFMR and SMAP Radiometer

Xiaohui Li [1], **Jingsong Yang** [1,2,*], **Guoqi Han** [3], **Lin Ren** [1,2], **Gang Zheng** [1,2], **Peng Chen** [1,2] **and Han Zhang** [1,2]

1   State Key Laboratory of Satellite Ocean Environment Dynamics, Second Institute of Oceanography, Ministry of Natural Resources, Hangzhou 310012, China
2   Southern Marine Science and Engineering Guangdong Laboratory (Zhuhai), Zhuhai 519082, China
3   Fisheries and Oceans Canada, Institute of Ocean Sciences, Sidney, BC V8L 4B2, Canada
*   Correspondence: jsyang@sio.org.cn

Abstract: Accurate information on tropical cyclone position, intensity, and structure is critical for storm surge prediction. Atmospheric reanalysis datasets can provide gridded, full coverage, long-term and multi-parameter atmospheric fields for the research on the impact of tropical cyclones on the upper ocean, which effectively makes up for the uneven temporal and spatial distribution of satellite remote sensing and in situ data. However, the reanalysis data cannot accurately describe characteristic parameters of tropical cyclones, especially in high wind conditions. In this paper, the performance of the tropical cyclone representation in ERA5 (European Centre for Medium-Range Weather Forecasts Reanalysis 5th Generation) is investigated and analyzed with respect to IBTrACS (International Best Track Archive for Climate Stewardship) during the period 2018–2020. Comparisons demonstrate that ERA5 winds significantly underestimate the maximum wind speed during the tropical cyclones (>30 m/s) compared to those provided by IBTrACS. An effective wind reconstruction method is examined to enhance tropical cyclone intensity representation in reanalysis data in 94 cases of 31 tropical cyclones 2018–2020. The reconstructed wind speeds are in good agreement with the SFMR (Stepped Frequency Microwave Radiometer) measured data and SMAP (Soil Moisture Active Passive) L-band radiometer remotely sensed measurements. The proposed wind reconstruction method can effectively improve the accuracy of the tropical cyclone representation in ERA5, and will benefit from the establishment of remote sensing satellite retrieval model and the forcing fields of the ocean model.

Keywords: tropical cyclone; cyclone intensity; wind field reconstruction; remote sensing; radiometer

1. Introduction

The tropical cyclone is one of the strongest synoptic events in the climate system of our Planet, causing severe damage and financial losses to the coastal community [1–4]. For example, Hurricane Katrina (2005) caused severe catastrophic damage and inflicted large loss of life, wetland and timber loss, and declines in fisheries and wildlife population along the Gulf Coast of Florida, Alabama, Mississippi and Louisiana [5–8]. Super Typhoon Rammasun (2014), which landed in Wenchang City, Hainan Province on 10 July 2014, was the strongest typhoon in China since 1949, resulting in the deaths of 88 people and financial losses of USD 7.2 billion [9]. Weaker storms, such as tropical depression, can also cause life loss and damage to vulnerable societies [2]. Therefore, it is very important to use the existing wind field data to understand the characteristics and behavior of tropical cyclones in order to reduce their social, economic and environmental impacts.

In the last century, in situ observations mainly depended on meteorological stations, buoys, ships, and airplanes, providing valuable information such as wind and wave information during tropical cyclones [10,11]. However, it could not ensure the spatial

continuity of observation, and could not meet the needs of marine disaster monitoring and early warning, marine dynamic processes and climate research. The emergence of atmospheric reanalysis datasets overcomes these shortcomings and provides a unique opportunity for global climate change research [12–14]. Atmospheric reanalysis datasets, which originated in the 1980s, use assimilation technology to synthesize measured data and numerical simulation to obtain grid products with higher accuracy, which can provide complete spatial and temporal atmosphere and surface conditions to simulate the impacts on the upper ocean after the passage of tropical cyclones [15]. Accurate information on tropical cyclone position, intensity and structure is critical to storm surge prediction. Current operational analysis and reanalysis wind products are important, forcing data to simulate storm surges, such as National Centers for Environmental Prediction (NCEP) [16], European Centre for Medium-Range Weather Forecasts (ECMWF) Atmospheric Reanalysis [17], MERRA (Modern-Era Retrospective Analysis for Research and Applications) Atmospheric Reanalysis [18], JRA (Japan Meteorological Agency Atmospheric Reanalysis) [19], and CRA (China Meteorological Agency Global Atmospheric Reanalysis) [20]. Over the last few decades, a large number of in situ observations have been assimilated, making atmospheric analysis and reanalysis products more and more accurate with the progress of ocean in situ, remote sensing observation systems [21], and newly emerging coastal video monitoring systems [22].

The realistic representation of tropical cyclones in reanalysis is the main goal of a long-term reanalysis project [23]. Previous studies of tropical cyclones using reanalysis have included cyclone detection, center positioning, intensity evaluating, wind profile evaluating, estimation of the rain fields produced by cyclones, and so on. For example, in order to evaluate the accuracy of the reanalysis data in tropical cyclone simulation, Hatsushika et al. [23] addressed that the tropical cyclone detection rate in JRA-25 is higher than that in ERA-40. They further evaluated and analyzed the impact of wind profile retrievals on tropical cyclone representations in JRA-25 reanalysis [23]. Moreover, the tropical cyclones detection rate was further investigated and analyzed in several atmospheric analysis and reanalysis products, showing that JRA-25 has better performance throughout the period of 1979–2003 [24]. In addition, subtropical and hybrid tropical storms can be also identified in the atmospheric analysis and reanalysis, providing a complete dataset for weather disaster assessment and analysis [25,26]. Truchelut and Hart [27] used the advances in global reanalysis methods to quantify the possible existence of undocumented Atlantic warm-core cyclones in reanalysis data, and the results show that reanalysis model is a promising tool for identifying cyclones which are undetected by traditional surface observational networks. These studies provide guidance for using reanalysis data to analyze and study the mechanism of tropical cyclones. Jourdain et al. [21] assessed the cyclones center location, the maximum wind speed, and the radius of the maximum wind speed (RMW) in ERA-Interim (ECMWF Re-Analysis-Interim) and ECMWF atmospheric operational analysis, and pointed out that resolution enhancement greatly improved the accuracy of the maximum wind speed and RMW. Kim et al. [28] examined the veracity of the tropical cyclone by using MERRA-2 (MERRA, version 2) global atmospheric reanalysis over the global tropical cyclone basins, and the result demonstrates that the climatological-mean features of tropical cyclones can be reproduced and well captured by MERRA-2 reanalysis. Tropical cyclones are also accompanied by strong rainfall, which causes flooding and erosion [29]. Villarini et al. [30] estimated the rainfall associated with landfalling tropical cyclone. Studies have demonstrated the potential benefits of gridded, full-coverage, and long-term reanalysis data for tropical cyclones identification, monitoring and analysis. Additionally, reanalysis data are useful not only for climatological research, but also for boundary conditions in the ocean hydrodynamic model [23,31–35].

However, there are still some gaps in the application of reanalysis data in tropical cyclones identification. Hodges et al. [2] systematically evaluated the ability of six reanalysis products (ERA-Interim, JRA-25, JRA-55, NCEP, MERRA, MERRA-2) to identify and track typhoons throughout the period 1979–2012, showing that tropical cyclone intensities

are significantly underestimated in the reanalysis compared to the best-track archive. This phenomenon has also been mentioned in previous studies [14,36–38]. It directly affects the accuracy of storm surge modeling [39]. Dullaart et al. [40] examined the performance of global surge simulation forced by the climate reanalysis datasets, and showed that the accuracy of storm surge simulation depends on whether the reanalysis data can accurately describe the intensities of tropical cyclones (10 m winds and mean pressure). In order to overcome the problem of underestimating tropical cyclone intensities via reanalysis data, the meteorological forcing derived from parametric tropical cyclone models is often applied to drive storm surge models [41,42], such as a symmetric wind model—Holland (1980) [43]—some asymmetric wind field models (such as the generalized asymmetric Holland model, GAHM [44], the Willoughby model [45] and the Ueno model [46]). In addition, the Hurricane wind (H*wind) [47] and Weather Research and Forecasting for Hurricanes (HWRF) models [48] are also effective when it comes to improving the quality of typhoon wind field and further improving the accuracy of storm surge simulation. These studies have shown that the wind output from the parametric tropical cyclone model or atmospheric model can reconstruct or reproduce tropical cyclone intensities and structures similar to observations.

In terms of improving the representation of tropical cyclone intensity in the reanalysis data, an effective typhoon reconstruction method has been proposed to minimize the errors in the wind field between the reanalysis and observations . The reconstructed wind fields have been applied to force a storm surge model, and the simulated results are significantly improved compared to the satellite altimeter and independent tide-gauge [49]. One of the advantages of this method is that it can be easily used to revise the typhoon wind fields based on the distance to typhoon center, RMW, and empirical ratio parameter, to further study the effects of these factors on the storm surge modeling. Recently, this typhoon reconstruction method was applied to reconstruct wind fields based on the Global Navigation Satellite System-Reflectometry (GNSS-R) coastal winds to improve the quality of ECMWF winds during typhoon Utor 2013, and the error between the surge model and tide gauge observations reduced by 30.5% [50]. Typical typhoon cases have been chosen to prove the potential of the proposed reconstruction method for improving tropical cyclone intensity representation in reanalysis data.

However, this method only uses buoy (single point) data to verify its effectiveness, and it is applied to a small number of statistical cases only. In this paper, we estimate the typhoon structure representation in ERA5 (ECMWF Reanalysis 5th Generation) using the best-track dataset, SFMR (Stepped Frequency Microwave Radiometer) data, and SMAP (Soil Moisture Active and Passive) L-band radiometer data during the period from 2018 to 2020. The premise of this method is that reanalysis can accurately reproduce the asymmetric structure of tropical cyclones, so the next step is to reconstruct the typhoon wind field for the case where the reanalyzed wind speed underestimates the measured data. Subsequently, the accuracy before and after wind reconstruction is assessed under different intensities. Compared to the wind profiles data from SFMR and wind distributions from SMAP radiometer, the accuracy of the intensity and typhoon structure after wind reconstruction is obtained. Finally, the advantages and disadvantages of this method are discussed, and conclusions are drawn.

2. Materials and Methods

2.1. ERA5

The fifth-generation atmospheric reanalysis data (https://www.ecmwf.int, accessed on 1 January 2022) within the Copernicus Climate Change Service (C3S) is adapted for validation and wind reconstruction in this study, which has a time resolution of 1 h and a spatial resolution of 31 km at the equator. ERA5 reanalysis is generated by assimilating the model prediction data with the measured data using the ECMWF Integrated Forecasting System (IFS), providing more physical parameters than ERA-Interim, such as wave height, wave direction and swell [17]. The historical wind field observation datasets are assimilated

to obtain a higher-precision product, including AMSR-E (Advanced Microwave Scanning Radiometer for the Earth Observing System), AMSR2 (Advanced Microwave Scanning Radiometer 2), GMI (Greenhouse Gases Monitoring Instrument), SSM/I (Special Sensor Microwave/Imager), MVIRI (Meteosat Visible and InfraRed Imager), SEVIRI (Spinning Enhanced Visible and Infrared Imager), GOES (Geo-Stationary Operational Environmental Satellite), GMS (Geostationary Meteorological Satellite), MTSAT (Multi-function Transport Satellite), AHI (Advanced Himawari Imagers), AVHRR (Advanced Very-High-Resolution Radiometer), MODIS (Modern Resolution Imaging Spectroradiometer), SeaWinds satellite data and in situ data (weather station, buoy, ship survey and airborne). The gridded ERA5 reanalysis data effectively make up for the uneven temporal and spatial distribution of satellite data and in situ data, and play a very important role in the establishment of remote sensing satellite retrieval model and the forcing fields of ocean model.

2.2. IBTrACS

IBTrACS (International Best Track Archive for Climate Stewardship) data, which provide locations and intensity for global tropical cyclones, are used to evaluate the representation of tropical cyclones in ERA5. The IBTrACS v04r00 spans from the 1840s to the present, generally providing data at 3 h intervals, which is the most recently released, global best-track dataset for tropical cyclones, produced by merging various reports from multiple agencies produced by the U.S. National Center for Climate Data (NCDC, https://www.ncdc.noaa.gov/ibtracs/index.php?name=ib-v4-access, accessed on 1 January 2022) [51]. There are two primary variables, including storm center of circulation and maximum sustained wind speed provided by the US agency. The storm center of circulation is the most important parameters of tropical cyclones, including the position of longitude and latitude (hereafter referred to as tropical cyclone position). The intensity of a cyclone is very important for disaster early warning. According to 1 min wind speeds [52], tropical cyclones can be classified as Tropical Depression, Tropical Storm, Category 1, Category 2, Category 3, Category 4, and Category 5, as shown in Table 1.

Table 1. Tropical systems classified based on the wind speed provided by the US agency wind speed [52].

Intensity	1 Min Wind Speeds (Knots)	Flag
Tropical Depression	Wind < 34	−1
Tropical Storm	34 < Wind < 64	0
Category 1	64 ≤ Wind < 83	1
Category 2	83 ≤ Wind < 96	2
Category 3	96 ≤ Wind < 113	3
Category 4	113 ≤ Wind < 137	4
Category 5	Wind ≥ 137	5

2.3. SFMR

The National Oceanic and Atmospheric Administration (NOAA)/Hurricane Research Division's SFMR is a new generation of airborne remote sensing instrument used to estimate the ocean surface brightness temperature at six frequencies between 4.6 and 7.2 GHz in hurricanes [53,54]. The sea surface winds along the flight track are then retrieved according to a function between wind speed and these brightness temperatures [55]. The retrieval accuracy of revised SFMR surface wind speeds is improved within ∼3.9 m/s root-mean-square error (RMSE) of the collocated observed dropsonde ones [56]. The wind profile of tropical cyclones can be obtained by SFMR, providing an important reference for verifying the reconstructed wind field in this study.

2.4. Methodology

The methodology is illustrated in Figure 1. First, tropical cyclones representation is evaluated within ERA5 reanalysis data, including tropical cyclone position and maximum

sustained wind speed. According to the track data provided by the US agency in IBTrACS, the location of the lowest wind speed in ERA5 within 150 km from the center of the best track is taken as the cyclone center (position of longitude and latitude). A similar method is also used to extract the tropical cyclone eye location from remote sensing data and compare it with the best-track data [57]. The geodesic distance between the cyclone center and the location of maximum wind speed in ERA5 is regarded as the RMW of a tropical cyclone, used as an indicator of tropical cyclone eye size [58]. The tropical cyclones detection method is used to identify and extract the characteristic parameters of tropical cyclones based on IBTrACS data. The criteria for identification and collocating are the following:

(1) The tropical cyclone must be named in IBTrACS; "Not_named" cyclones are ignored.
(2) All invalid values are ignored in the tropical cyclone position of longitude and latitude, maximum sustained wind speed and RMW variables provided by IBTrACS.
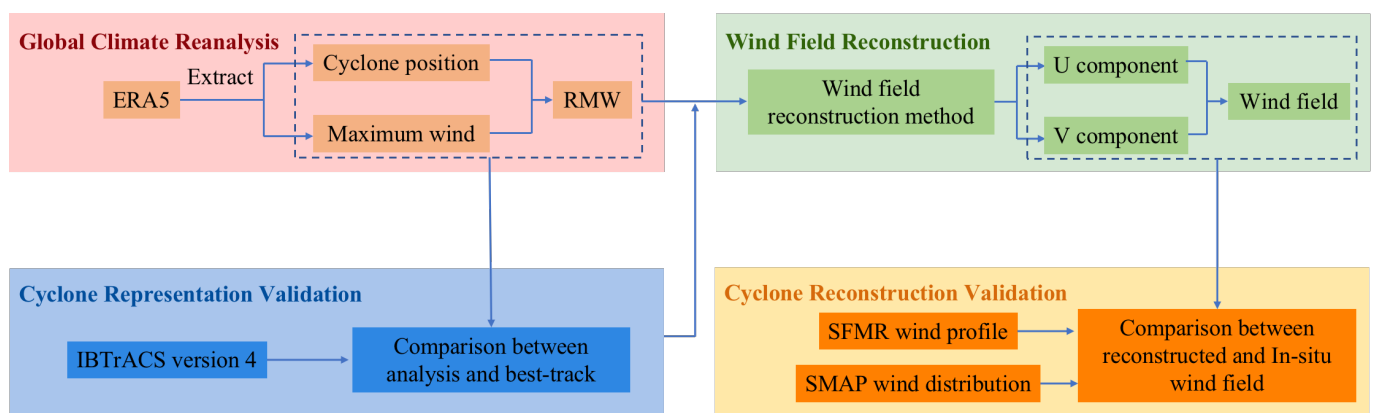(3) The intensity level of tropical cyclones provided by IBTrACS should be higher than Tropical Depression.

Figure 1. Flowchart of the research framework showing the ERA5 datasets (top left), tropical cyclones representation validation (bottom left), wind field reconstruction (top right) and validation (bottom right).

Second, the key parameters of tropical cyclone are compared against those of IBTrACS to examine the characteristics and performance of the tropical cyclones representation in ERA5. Position deviation is defined as the difference between the track data provided by IBTrACS and the tropical cyclone position evaluated by ERA5. The RMSE of the maximum wind speed within ERA5 is calculated according to the track data provided by IBTrACS. According to the relationship between IBTrACS and ERA5, the maximum wind speed underestimation in ERA5 may be revised. So, the ratio of the maximum wind speed (*Maxwind_BT*) provided by IBTrACS to that estimated by reanalysis (*Maxwind_BG*) is adopted in this study. The specific calculation is shown in Equation (1).

$$\text{ratio} = \frac{Maxwind\_BT}{Maxwind\_BG} \tag{1}$$

Subsequently, a typhoon wind field reconstruction method is used as shown in Equation (2) to reconstruct wind fields based on the characteristic parameters of tropical cyclones and distance correction parameter. To evaluate the performance of the reconstructed wind fields, we compare the reconstructed wind fields with the wind profile

from SFMR and wind distributions from SMAP, respectively. Finally, the conclusion and discussion are drawn.

$$
V(r) = \begin{cases}
(\dfrac{r}{RMW} \times \text{ratio} + \dfrac{RMW - r}{RMW}) \times V_{BG}, & 0 \leq r < RMW \\[4mm]
(\dfrac{r - RMW}{3RMW} + \dfrac{4RMW - r}{3RMW} \times \text{ratio}) \times V_{BG}, & RMW \leq r < 4RMW \\[4mm]
V_{BG}, & r \geq 4RMW
\end{cases}
\tag{2}
$$

where V is the reconstructed wind speed, r is the distance from the tropical cyclone center, V_{BG} is the wind speed of the background field, and ERA5 wind field is used in this study. In addition, the forecast or theoretical wind field can be also regarded as the background field. ratio is the key parameter for wind fields reconstruction. In order to clearly describe each variable, Table 2 gives its relevant details, including the description of each variable and its units.

Table 2. Description of each variable used in the proposed method.

Variable	Unit	Description
$V(r)$	m/s	Reconstructed wind speed
r	km	Distance from the tropical cyclone center
V_{BG}	m/s	Background field from ERA5
RMW	m/s	Radius of the maximum wind speed
ratio	–	Empirical parameter

Our previous work attempted to revise the reanalysis wind field by using the ratio = 1.1, 1.2, 1.3, 1.4, 1.5 during the period from 9 October to 11 October 1994 [49]. The reconstructed wind speeds agree closely with those observed at the meteorological station with ratio = 1.3, which are used as the forcing wind to simulate a storm surge induced by typhoon Seth. Furthermore, the storm surge model results agree with tide-gauge and altimetric data simultaneously when ratio = 1.3. In another study, we estimated the ratio based on the coastal GNSS-R measurements and ECMWF winds. The results show that the average RMSE of the surge model has been reduced by 30.5% from 24.3 cm with the ECMWF winds to 16.9 cm with the reconstructed winds [50]. These previous research results illustrate the potential benefits of an accurate reconstruction of the wind fields for storm surge simulations.

2.5. Evaluation Metrics

In this study, three metrics are chosen to evaluate the performance of the ERA5 representation in tropical cyclones and the proposed model, including the mean deviation (or bias), the root-mean-square error (RMSE) and correlation coefficient (R), which are defined as

$$
\text{bias} = \frac{1}{n} \sum_{i=1}^{n} (X_i - Y_i)
\tag{3}
$$

$$
\text{RMSE} = \sqrt{\frac{1}{n} \sum_{i=1}^{n} (X_i - Y_i)^2}
\tag{4}
$$

$$
\text{R} = \frac{\sum_{i=1}^{n} (X_i - \overline{X})(Y_i - \overline{Y})}{\sqrt{\sum_{i=1}^{n} (X_i - \overline{X})^2 \sum_{i=1}^{n} (Y_i - \overline{Y})^2}}
\tag{5}
$$

where X represents the evaluated data, Y represents the reference data, n is the number of total matchups, $\overline{X}$ is the mean of the evaluated data and $\overline{Y}$ is the mean of the reference data.

3. Results

3.1. Validation and Uncertainty Estimate

To assess the performance of the ERA5 representation with respect to IBTrACS, we calculate the position deviation of global tropical cyclones for the period from 2018 to 2020. There are 271 tropical cyclones used to evaluate the tropical cyclones representation in ERA5. According to the matching results, there are 8636 cases for these three years, including 1587 cases in tropical depression, 4099 cases in tropical storm, 1141 cases in Category 1, 646 cases in Category 2, 556 cases in Category 3, 461 cases in Category 4 and 146 cases in Category 5.

3.1.1. Position Uncertainty

Figure 2 shows the histogram of position deviation between the representation in ERA5 and IBTrACS. It can be seen that the deviation is mainly in 10~60 km. Furthermore, when the position deviation exceeds 30 km, the number of its distributions quickly decreases with increasing deviation. The bias of the tropical cyclone center is 43.8 km in ERA5 with respect to IBTrACS. In general, the results illustrate that the tropical cyclone center position estimated by ERA5 is in good agreement with IBTrACS.
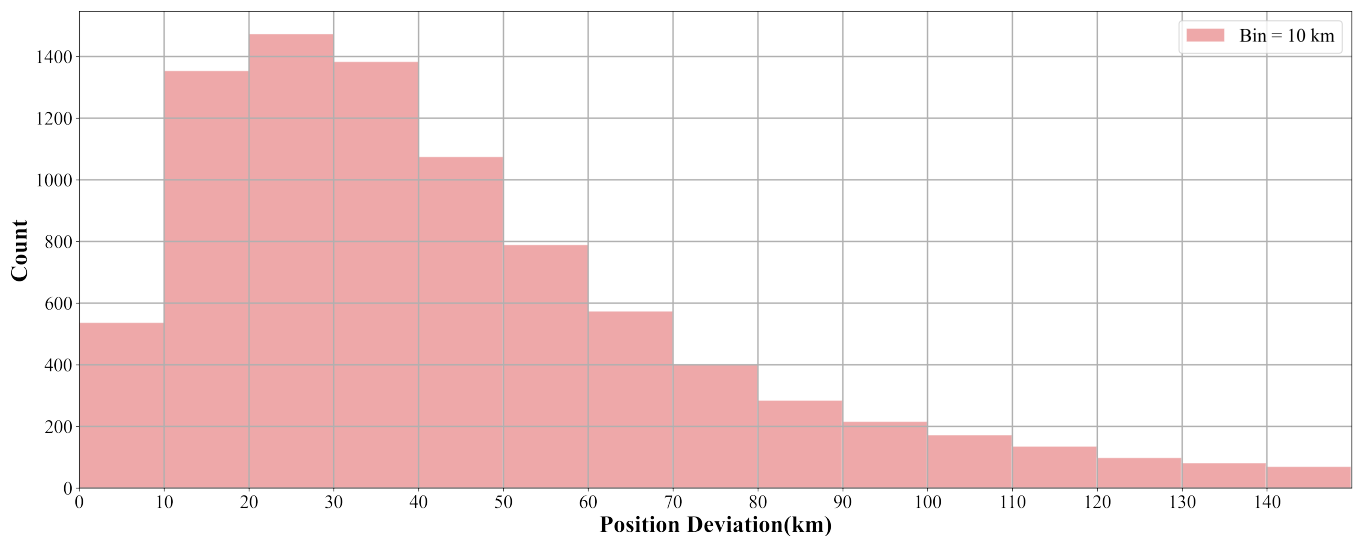

Figure 2. Histogram of position deviation of the representation in ERA5 with respect to IBTrACS.

The accuracy of the tropical cyclone center position estimated by ERA5 varies with the intensity of tropical cyclones. Position deviation in each tropical cyclone intensity category is investigated and analyzed according to the intensity provided by IBTrACS. Figure 3 shows the distribution of error bar in different tropical cyclone intensities. It can be seen that with the increase in the intensity of tropical cyclones, the accuracy of the typhoon center evaluated by ERA5 also increases. The number of samples in each tropical cyclone intensity will also affect the accuracy of its evaluation. Tropical storms have the largest number of samples. The number of Category 5 is 146, and this is sufficient to evaluate its accuracy.

3.1.2. Comparison of Maximum Wind Speed between IBTrACS and ERA5

To facilitate comparison, the maximum wind speeds provided by IBTrACS in knots are converted to sea surface wind speeds in meters per second. Figure 4 shows the scatter plot of the maximum wind speeds between IBTrACS and ERA5. It can be seen that the maximum wind speeds estimated by ERA5 are less than 40 m/s. Nevertheless, the collaborated IBTrACS maximum wind speeds reach up to 80 m/s. The results demonstrate that tropical cyclones' intensity has been strongly underestimated in ERA5 compared to these provided by IBTrACS.
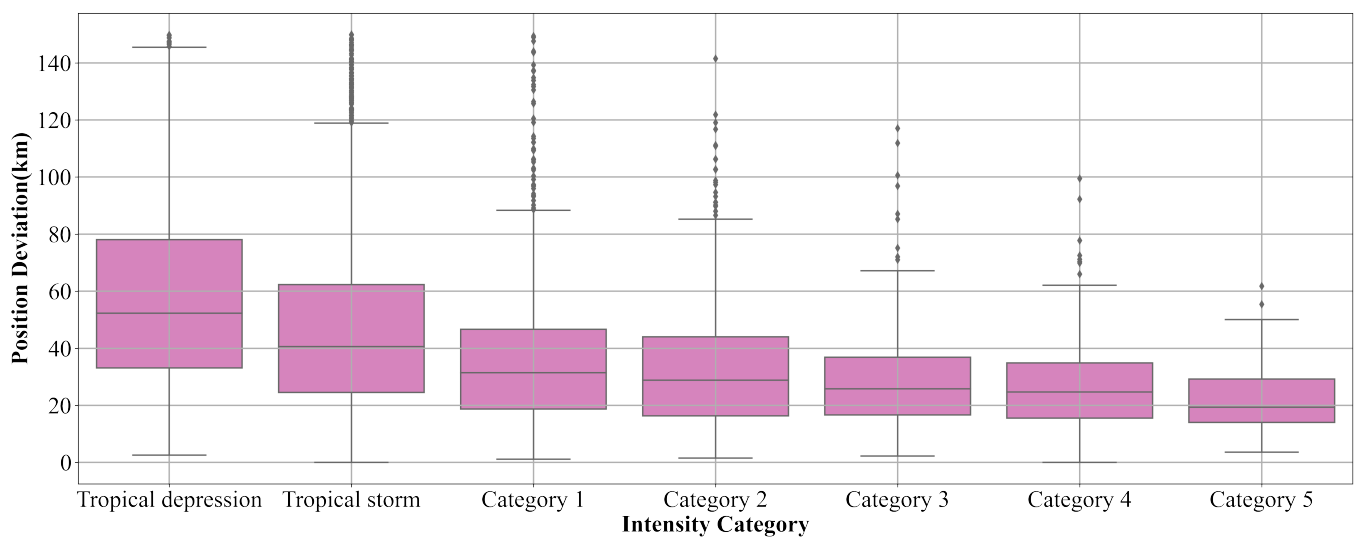
Figure 3. Box and whiskers plots of position deviation among each intensity categories.
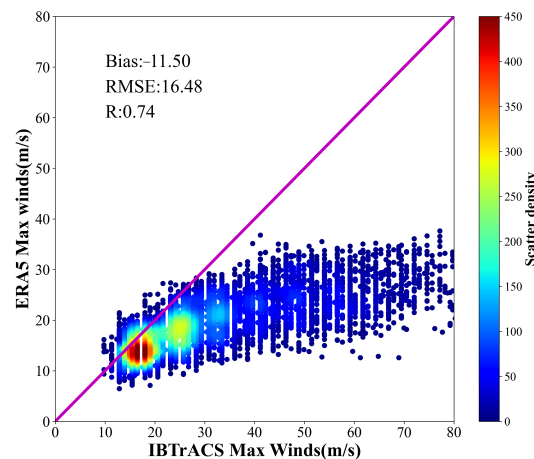

Figure 4. Scatter plot of maximum wind speeds between IBTrACS and ERA5 during the period 2018–2020. The color scale is the number of data points.

Schenkel and Hart [14] pointed out that although ERA5 is unable to resolve the tropical cyclones intensity, it is still of some use due to the significant correlation coefficients between best-track data and reanalysis. Therefore, we can revise the problem of underestimation of maximum wind speeds in ERA5 according to the relationship between IBTrACS and ERA5.

3.2. Wind Fields Reconstructed by Proposed Method

Comparison of the maximum wind speed between IBTrACS and ERA5 demonstrates that ERA5 strongly underestimates the intensity of tropical cyclones . To solve this problem, the wind speed of tropical cyclones is reconstructed according to the proposed reconstruction method. The tropical cyclones are determined by the SFMR during the period 2018–2020. Table 3 gives details of the name of the tropical cyclone, the reconstructed time of the wind fields and its intensity. There are 31 tropical cyclones for these three years, including Beryl, Chris, Florence, Gordon, Isaac, Kirk, Michael, Olivia and Rosa in 2018, and Barry, Dorian, Humberto, Ivo, Jerry, Karen, Lorenzo and Nestor in 2019, and Arthur, Beta, Cristobal, Delta, Douglas, Eta, Gamma, Hanna, Isaias, Laura, Paulette, Sally, Teddy and Zeta in 2020. As can be seen from Table 3, there are 94 cases, including 1 tropical depression, 46 tropical storm, 22 Category 1, 13 Category 2, 6 Category 3, 3 Category 4. The remaining two of Beryl in 2018 and Nestor in 2019 are miscellaneous disturbances.

These cases are determined based on the wind profile of the cyclones captured by SFMR, which is convenient for the next verification.

Table 3. Tropical cyclones for the reconstruction and validation during the period 2018–2020.

Name	Reconstruction Time	Intensity	Name	Reconstruction Time	Intensity
Beryl	20180708 12:00	–	Lorenzo	20190928 18:00	Category 4
Chris	20180708 18:00	Tropical storm	Nestor	20191018 12:00	–
Florence	20180912 15:00	Category 3	Arthur	20200518 12:00	Tropical storm
Florence	20180913 12:00	Category 2	Beta	20200921 12:00	Tropical storm
Florence	20180913 21:00	Category 2	Beta	20200921 15:00	Tropical storm
Florence	20180914 06:00	Category 2	Cristobal	20200602 15:00	Tropical storm
Florence	20180914 09:00	Category 1	Cristobal	20200603 12:00	Tropical storm
Gordon	20180904 18:00	Tropical storm	Delta	20201008 12:00	Category 2
Isaac	20180912 15:00	Tropical storm	Delta	20201009 06:00	Category 3
Kirk	20180926 15:00	–	Delta	20201009 15:00	Category 2
Kirk	20180928 15:00	Tropical storm	Delta	20201009 18:00	Category 2
Michael	20181008 06:00	Tropical storm	Douglas	20200725 18:00	Category 2
Michael	20181008 12:00	Category 1	Douglas	20200726 21:00	Category 1
Michael	20181009 09:00	Category 2	Eta	20201101 18:00	Tropical storm
Olivia	20180911 21:00	Tropical storm	Eta	20201109 15:00	Tropical storm
Rosa	20180930 18:00	Category 1	Gamma	20201004 15:00	Tropical storm
Barry	20190711 09:00	Tropical storm	Hanna	20200724 15:00	Tropical storm
Barry	20190711 12:00	Tropical storm	Hanna	20200725 12:00	Category 1
Barry	20190712 12:00	Tropical storm	Hanna	20200725 18:00	Category 1
Barry	20190712 15:00	Tropical storm	Isaias	20200730 15:00	Tropical storm
Barry	20190712 18:00	Tropical storm	Isaias	20200731 06:00	Category 1
Barry	20190713 15:00	Category 1	Isaias	20200801 21:00	Tropical storm
Dorian	20190827 12:00	Tropical storm	Isaias	20200802 09:00	Tropical storm
Dorian	20190827 15:00	Tropical storm	Isaias	20200802 12:00	Tropical storm
Dorian	20190827 18:00	Tropical storm	Isaias	20200803 12:00	Tropical storm
Dorian	20190829 15:00	Category 1	Isaias	20200803 15:00	Tropical storm
Dorian	20190831 15:00	Category 4	Laura	20200824 12:00	Tropical storm
Dorian	20190902 21:00	Category 4	Laura	20200825 12:00	Category 1
Dorian	20190903 15:00	Category 3	Laura	20200825 15:00	Category 1
Dorian	20190904 09:00	Category 2	Paulette	20200913 12:00	Category 1
Dorian	20190904 18:00	Category 2	Sally	20200912 18:00	Tropical storm
Dorian	20190904 21:00	Category 3	Sally	20200913 12:00	Tropical storm
Dorian	20190905 18:00	Category 2	Sally	20200913 15:00	Tropical storm
Humberto	20190914 12:00	Tropical storm	Sally	20200913 18:00	Tropical storm
Humberto	20190915 18:00	Tropical storm	Sally	20200915 06:00	Category 1
Humberto	20190916 12:00	Category 1	Sally	20200915 15:00	Category 1
Humberto	20190918 12:00	Category 1	Sally	20200915 18:00	Category 1
Ivo	20190824 21:00	Tropical storm	Sally	20200916 09:00	Category 2
Jerry	20190920 15:00	Category 1	Teddy	20200917 15:00	Category 3
Jerry	20190921 03:00	Tropical storm	Teddy	20200921 12:00	Category 1
Jerry	20190921 12:00	Tropical storm	Teddy	20200922 15:00	Category 2
Jerry	20190923 12:00	Tropical storm	Teddy	20200922 21:00	Category 1
Jerry	20190924 12:00	Tropical storm	Zeta	20201025 06:00	Tropical storm
Jerry	20190924 15:00	Tropical storm	Zeta	20201025 21:00	Tropical storm
Karen	20190923 12:00	Tropical depression	Zeta	20201026 06:00	Category 1
Karen	20190924 15:00	Tropical storm	Zeta	20201026 18:00	Category 1
Karen	20190925 18:00	Tropical storm	Zeta	20201028 21:00	Category 3

From the proposed method, the accurate reconstruction of a cyclone wind field depends on the accurate estimation of its key parameters and ratio parameter. In order to ensure the correctness of the cyclone position, the center position provided by IBTrACS is used for wind field reconstruction. The proposed reconstruction method takes ERA5 data as the background field and its premise is that ERA5 can reproduce the asymmetric structure of tropical cyclones. So the geodesic distance between the cyclone center and

the location of maximum wind speed in ERA5 is regarded as the RMW of a tropical cyclone. Then, the ratio parameter of 94 cases is estimated according to Equation (1). Finally, the wind fields of 31 tropical cyclones are reconstructed according to the key parameters and ratio parameter at each time.

3.3. Validation of Wind Fields between SFMR and Reconstruction

The wind fields within four times RMW in 94 cases of 31 tropical cyclones are reconstructed based on the proposed reconstruction method. In order to ensure the accuracy of SFMR wind speed data, we have carried out quality control and eliminated abnormal data when the flag is nonzero. To evaluate the wind speed and typhoon structure of the reconstructed wind fields, we selected the measurements of SFMR flight trajectory passing through the typhoon center (within twice RMW and 30 min). Then, the collocated data from the reconstructed wind fields are linearly interpolated to the SFMR flight trajectory. Finally, the accuracy of the reconstructed wind fields can be evaluated in bias, RMSE and correlation coefficient (R) with respect to SFMR wind measurements.

Figure 5 shows the comparison of the scatter plots before and after tropical cyclone wind field reconstruction relative to SFMR. Figure 5a illustrates the ERA5 winds underestimate in the high wind range compared to SFMR ones. The statistical comparisons show that the bias and RMSE of ERA5 winds are –6.06 m/s and 8.38 m/s, respectively. Those of reconstructed winds are –0.19 m/s and 7.83 m/s, respectively. The wind difference between reconstructed and SFMR winds has improved significantly compared to that between ERA5 and SFMR winds.
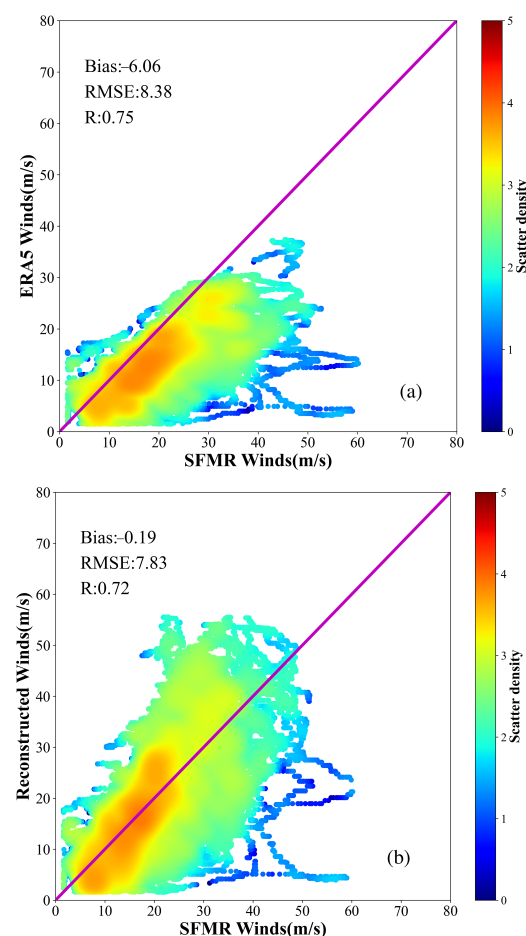

Figure 5. Scatter plots of wind speeds between SFMR and before and after reconstruction. The color scale is the common logarithm of the number of data points. (**a**) Comparison of wind speeds between SFMR and ERA5, (**b**) Comparison of wind speeds between SFMR and reconstruction.

As we all know, a tropical cyclone can cause storm surge disasters before and after its landing. Therefore, it is of great significance to accurately describe the wind field distribution. However, our research shows that ERA5 underestimates winds compared to IBTrACS. This can also be seen from the comparison between ERA5 and SFMR, as shown in Figure 5a. Tropical cyclone wind fields are reconstructed using the proposed method in 94 cases of 31 tropical cyclones. Then, compared to SFMR wind measurements, it can be seen that the wind speeds during Florence in 2018, Dorian in 2019 and Delta in 2020 have increased significantly, which is more consistent with the SFMR shown in Figures 6–8.

On the eve of tropical cyclone Florence in 2018 and Delta in 2020, SMFR observed the wind profile of these tropical cyclones, as shown in Figure 6. It can be seen that the maximum of ERA5 wind speeds is less than 30 m/s both in Florence in 2018 and Delta in 2020. The profiles of the reconstructed winds are more consistent with these of SFMR. Moreover, maximums of reconstructed wind speeds exceed 40 m/s both Florence in 2018 and Delta in 2020. The reconstructed wind fields distribution completely retain the asymmetric structure of reanalysis data, and the intensities of Florence and Delta have significantly improved.
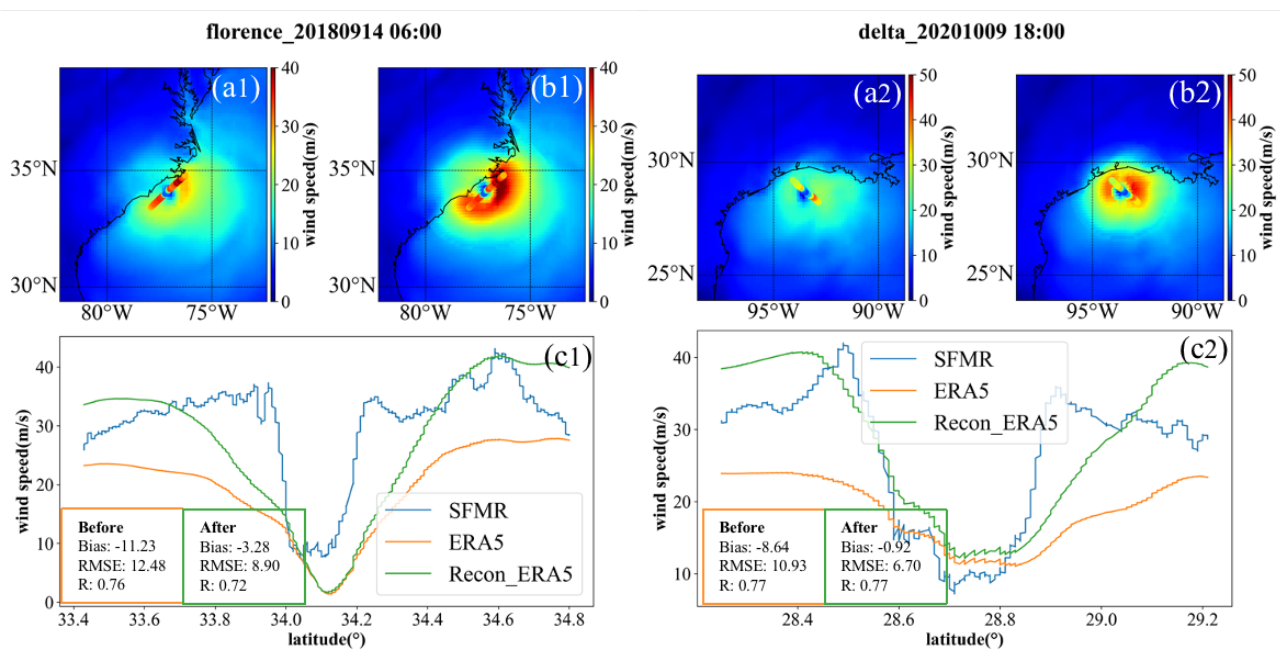

Figure 6. Comparison of wind field (**a1**–**b2**) and profile (**c1**,**c2**) before and after tropical cyclone reconstruction at Florence in 2018 and Delta in 2020.

Figure 7 shows the results of wind fields and profiles before and after the wind field reconstruction when Dorian is close to the nearshore. At 09:00 (UTC) on 4 September 2019, compared to ERA5 winds, the profile of the reconstructed winds was more consistent with that of SFMR. On the contrary, at 12:00 (UTC) on 24 September 2019, Figure 8 shows the wind field and profile before and after wind field reconstruction when Jerry was on the open sea; it can be seen that the maximum wind speed increased and the profile of the reconstructed winds agreed well with SFMR measurements.

What is more interesting is that SFMR focused on observing the wind speed inside Dorian at 21:00 (UTC) on 4 September 2019, and the reconstructed wind speed is in good agreement with the SFMR wind speed. In addition, at 15:00 (UTC) on 24 September 2019, it should be pointed out that the wind speed around the RMW of Jerry was observed by SFMR, as shown in Figure 8; the results seem to be in agreement with SFMR measurements.
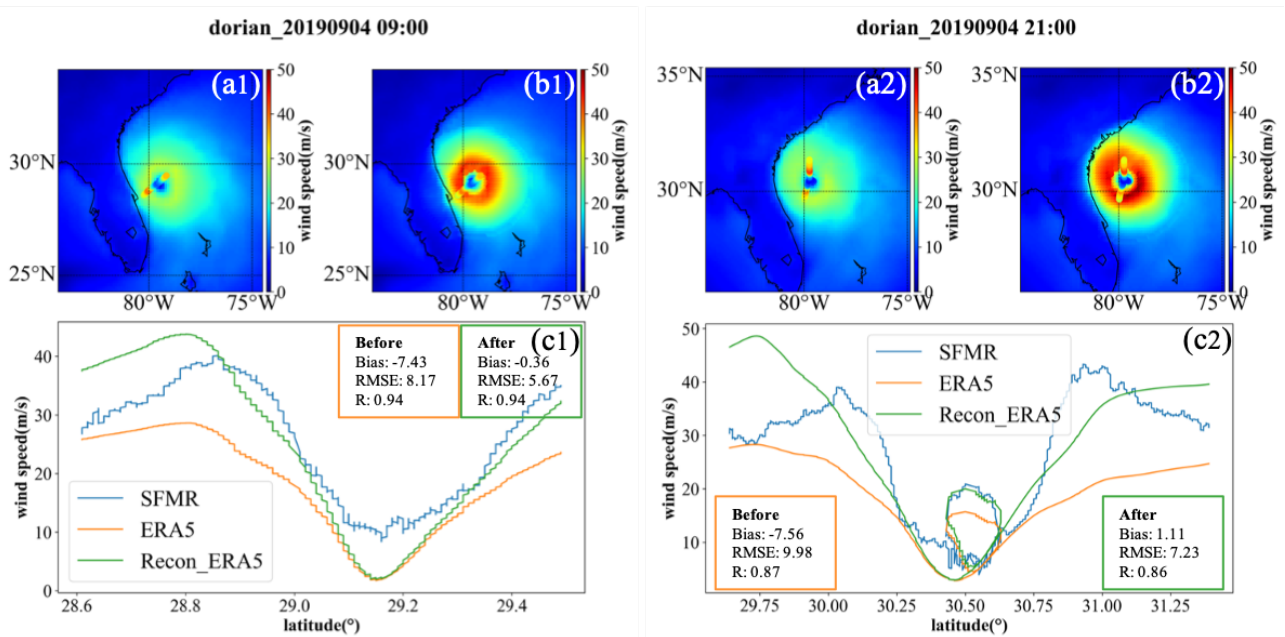
Figure 7. Comparison of wind field (**a1**–**b2**) and profile (**c1**,**c2**) before and after tropical cyclone reconstruction at Dorian in 2019.
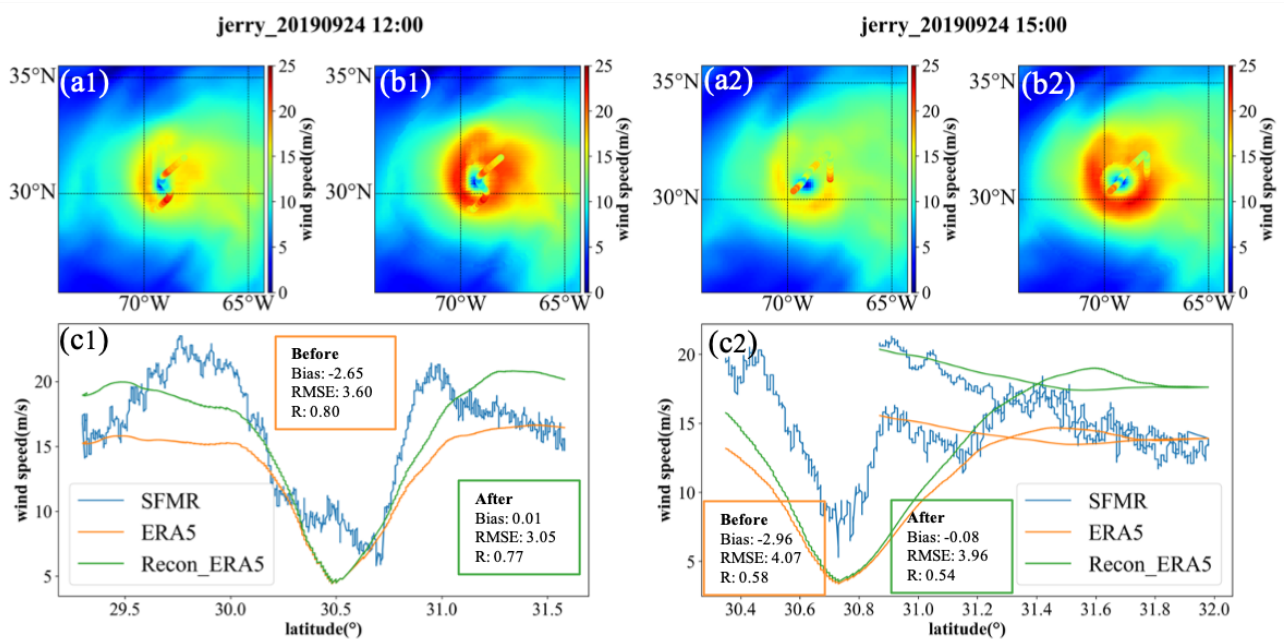

Figure 8. Comparison of wind field (**a1**–**b2**) and profile (**c1**,**c2**) before and after tropical cyclone reconstruction at Jerry in 2019.

In general, the proposed method can effectively improve the wind speed inside the tropical cyclone, around the RMW and in its periphery, whether the tropical cyclone is in the open sea or near the shore. Comparisons demonstrate that the reconstructed wind speeds are in good agreement with the SMFR measured data. The effectiveness of this method is also proved by 94 cyclone cases during 2018–2020, which further makes up for the underestimation of cyclone intensity by atmospheric reanalysis data.

3.4. Validation of Wind Fields between SMAP and Reconstruction

In this section, we compare the reconstructed wind speeds with wind measurements from the SMAP L-band radiometer in tropical cyclones, which are produced by using

algorithms developed for high wind conditions [59,60]. The accuracy of SMAP under tropical cyclones conditions is confirmed and compared with HWRF, with the standard deviation below 4 m/s for high wind between 10 and 60 m/s [61]. This provides valuable data for evaluating the wind field verification after reconstruction.

In order to accurately assess the reconstructed wind speeds based on the proposed method, it is necessary to collocate with the SMAP L-band radiometer measurements that are observed within a short time window and within an adjacent grid point as closely as possible. Because of this, the wind speeds from the SMAP L-band radiometer are obtained by a temporal and spatial window within 1 h and 12.5 km. The SMAP L-band radiometer wind speed product includes both ascending and descending satellite passes in the daily Level 3 file from Remote Sensing System (available at www.remss.com/missions/smap, accessed on 1 June 2022).

For comparison with SMAP, wind speed measurements during a total of 31 tropical cyclones (Table 3) are selected from the SMAP L-band radiometer. In order to illustrate the accuracy of the reconstructed wind field, a scatter diagram for all tropical cyclone cases is more effective than two-dimensional wind speed distribution. Figure 9 gives the scatterplot and statistics for before (a) and after (b) reconstructed wind speed versus the collocated SMAP high wind speed. It can be seen that ERA5 winds have a bias of −2.02 m/s and a RMSE of 4.04 m/s. The statistical analysis of the correlation coefficient confirms the very good correlation between ERA5 winds and radiometer SMAP. However, ERA5 winds are lower than those from the SMAP L-band radiometer at wind speeds above 20 m/s. Relative to SMAP, it also indicates that the phenomenon of ERA5 underestimates that high wind speeds still exist. On the other hand, the reconstructed winds are in good agreement with the SMAP measured data during tropical cyclones, with a small bias of 0.77 m/s, small RMSE of 3.34 m/s, and correlation coefficient of 0.93.
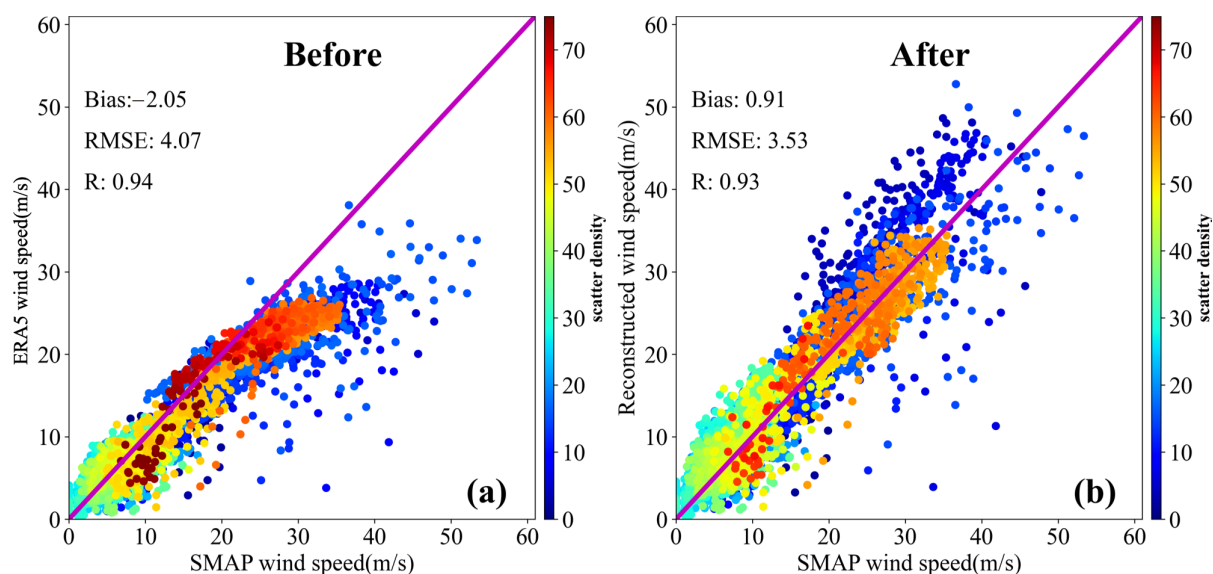

Figure 9. Comparison of wind field between before (**a**) and after (**b**) tropical cyclone reconstruction during the period from 2018 to 2020. The color scale is the number of data points.

The wind profile of a tropical cyclone is compared with that of a SFMR, and the results show that they are in good agreement. Satellite remote sensing can observe a two-dimensional wind field during tropical cyclones. Here, we show the comparison between the reconstructed wind field and SMAP measured data to further confirm the effectiveness of the reconstruction method. Figure 10 displays a comparison in wind distribution between the before (b)/after (c) reconstructed wind speed and SMAP (a) high wind speed within four times RMW at 21:00 (UTC) 22 September 2020 during Hurricane Teddy. From the spatial distribution of the wind field, the reconstructed wind field is more consistent with SMAP measured data for Hurricane Teddy. The scatterplot of the

before/after reconstructed wind speed versus SMAP for Hurricane Teddy is similar to the one for overall cases, as shown in Figure 10d, with ERA5 underestimating winds above 20 m/s. The statistical analysis of the reconstructed wind speed and SMAP shows good consistency between the two winds, with a small bias of −0.30 m/s, a small RMSE of 2.99 m/s, and a high correlation coefficient of 0.82, giving confidence in the proposed method for wind field construction during tropical cyclones.
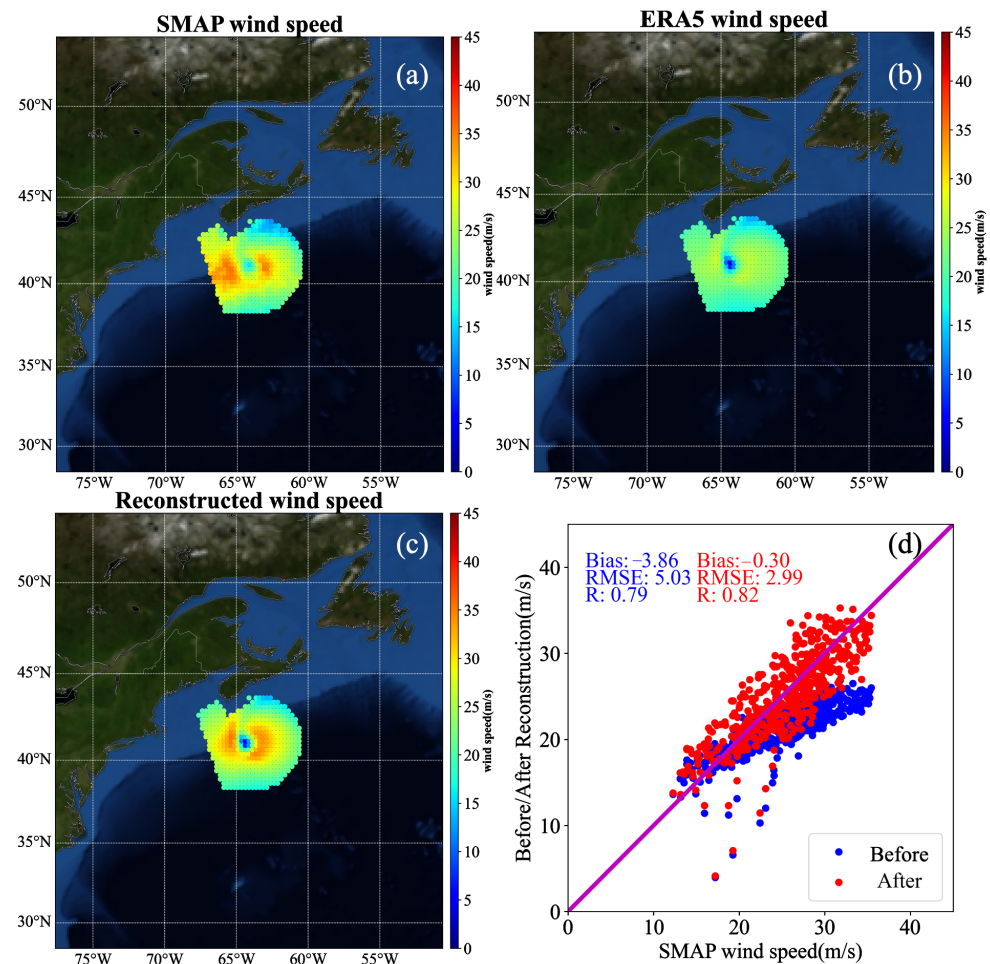

Figure 10. Wind distribution of Hurricane Teddy at 21:00 (UTC) 22 September 2020 in SMAP (**a**) and collocated with the before (**b**) and after (**c**) reconstructed wind speed within four times RMW based on the proposed method. (**d**) Scatterplot and statistics for the before (blue scatters) and after (red scatters) reconstructed wind speed versus the collocated SMAP high wind speed at 21:00 (UTC) 22 September 2020 during Hurricane Teddy.

4. Discussion

We use the IBTrACS best-track dataset to estimate the typhoon structure representation in ERA5. It is found that the accuracy of tropical depression has larger position deviation. For the explanation of the variability of position deviation in each intensity category, the ERA5 maybe unable to properly reproduce the impact of tropical cyclone beta gyres on storm motion when its intensity is small [14]. In addition, Zehnder [62] pointed out that the complex topography also affects the tropical cyclone tracks and Schenkel and Hart [14] indicated that the reanalysis cannot adequately resolve this complex topography, resulting in position deviation due to the relative lacking of topographical observations. Considering the impact of storm waves on the coasts induced by tropical cyclones, short-wave perturbation can influence the position and thermal structure of the cyclone, producing an operational ensemble forecast via ECMWF [63,64].

In our previous work [49], we used the proposed reconstruction method to prove its effectiveness for a single tropical cyclone case, in which the absolute bias reduced from -2.8 m/s to -0.3 m/s, and RMSE was also reduced by 30% [49]. In this study, we used 94 cases belonging to cyclones with varied intensities to verify the effectiveness and feasibility of this method. Statistical analysis shows that the absolute bias can be significantly reduced from -6.06 m/s to -0.19 m/s. In addition, the accuracy can be improved by 13.2% in RMSE with respect to SMAP.

Although the proposed method can improve the tropical cyclones representation in ERA5, it is also assumed that ERA5 can reproduce the structure of the cyclone well . If the RMW estimated by ERA5 is quite different from the actual situation, the wind field may not be reconstructed accurately. As shown in Figure 11, although the asymmetry in ERA5 is similar to that observed by SFMR, the wind speed on the upper right of the cyclone center is larger, and that on the lower left is smaller. However, the cyclone size evaluated by ERA5 for Michael at 09:00 (UTC) on 9 October 2018 is larger than that of SFMR, resulting in a large difference in the wind profile between reconstruction and SFMR. It was also found that there is a difference between the cyclone center position from IBTrACS and SFMR, which also leads to inconsistency between the reconstructed winds near the cyclone center and the measured ones. At 12:00 (UTC) on 13 September 2020, Paulette was in the open sea. The cyclone center from IBTrACS and the reconstructed cyclone intensity (maximum wind speed exceeds 30 m/s) were almost consistent with those of SFMR. However, the RMW assessed by ERA5 was inaccurate, resulting in an inconsistency between the wind profile and the measured data. Therefore, when using the proposed method, it is necessary to evaluate the description of cyclone size and structure in reanalysis data, which will directly affect the accuracy of wind field reconstruction.
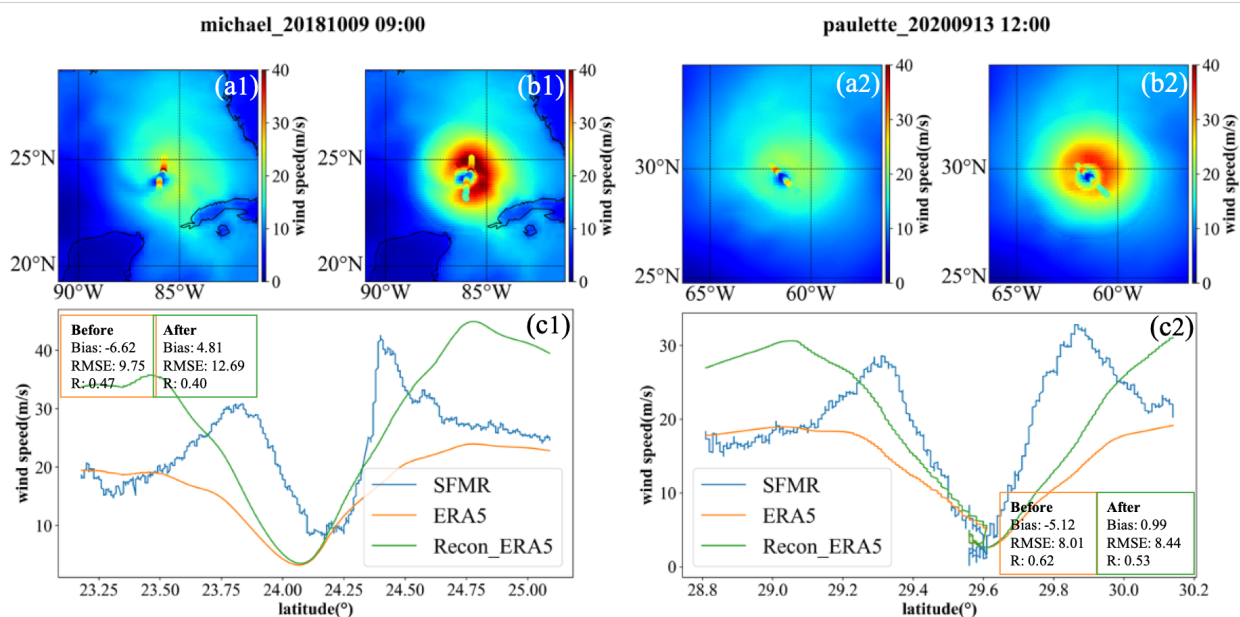

Figure 11. Comparison of field (**a1**–**b2**) and profile (**c1**,**c2**) before and after tropical cyclone reconstruction at Michael in 2018 and Paulette 2020.

5. Conclusions

The results of this study represent a comprehensive attempt to evaluate the tropical cyclone's center location and intensity (maximum wind speed) in the ERA5 dataset for the period from 2018 to 2020. It is found that ERA5 can reasonably reproduce the cyclone center when the temporal and spatial resolution is 1 h and 0.125°. However, the cyclone intensity is seriously underestimated compared to that provided by IBTrACS, SFMR and SMAP. A wind field reconstruction method is proposed to minimize the errors of the wind field between reanalysis and observations, which can reconstruct the wind field

within four times of RMW of tropical cyclones. For 94 cyclone cases during the period of 2018–2020, the comparison shows that the reconstructed wind field is closer to SFMR measurements, and the bias can be reduced from -6.06 m/s of ERA5 to -0.19 m/s after reconstruction. Compared to the wind profile observed by SFMR, it is found that the profile of the reconstructed wind field is more consistent with the measured data. Finally, the spatial distribution of the storm wind field is validated by the SMAP L-band radiometer, which confirms the improvement of tropical cyclone wind fields in the atmospheric reanalysis datasets using the proposed reconstruction method.

Author Contributions: Conceptualization, X.L., G.H. and J.Y.; methodology, X.L. and L.R.; software, X.L.; validation, X.L., G.Z. and P.C.; formal analysis, X.L. and H.Z.; investigation, X.L. and G.H.; writing—original draft preparation, X.L.; writing—review and editing, X.L., G.H. and J.Y. All authors have read and agreed to the published version of the manuscript.

Data Availability Statement: The ERA5 reanalysis dataset is freely distributed on https://www. ecmwf.int (accessed on 1 January 2022). The location and intensity for global tropical cyclones of IBTrACS are from https://www.ncdc.noaa.gov/ibtracs/index.php?name=ib-v4-access (accessed on 1 January 2022). The radiometer wind dataset is freely distributed on the Remote Sensing System website following pages: SMAP at https://www.remss.com/missions/smap/ (accessed on 1 June 2022).

Conflicts of Interest: The authors declare no conflicts of interest.

References

1. Price, J.F. Upper Ocean Response to a Hurricane. *J. Phys. Oceanogr.* **1981**, *11*, 153–175. [CrossRef]
2. Hodges, K.; Cobb, A.; Vidale, P.L. How Well are Tropical Cyclones Represented in Reanalysis Datasets? *J. Climate* **2017**, *30*, 5243–5264. [CrossRef]
3. Liu, Y.; Weisberg, R.H.; Zheng, L. Impacts of Hurricane Irma on the Circulation and Transport in Florida Bay and the Charlotte Harbor Estuary. *Estuar. Coast.* **2020**, *43*, 1194–1216. [CrossRef]
4. Zhang, H.; Liu, X.; Wu, R.; Chen, D.; Zhang, W. Sea Surface Current Response Patterns to Tropical Cyclones. *J. Mar. Sys.* **2020**, *208*, 103345. [CrossRef]
5. Sheikh, P.A. *The Impact of Hurricane Katrina on Biological Resources*; Technical Report; Congressional Research Service Report to Congress, RL33117; The Library of Congress: Washington, DC, USA, 2005.
6. Knabb, R.D.; Rhome, J.R.; Brown, D.P. Tropical Cyclone Report: Hurricane Katrina, August 23–30. 2005. *Fire Eng.* **2006**, *42*, 1–42.
7. Fritz, H.M.; Blount, C.; Sokoloski, R.; Singleton, J.; Fuggle, A.; Mcadoo, B.G.; Moore, A.; Grass, C.; Tate, B. Hurricane Katrina Storm Surge Reconnaissance. *J. Geotech. Geoenviron. Eng.* **2008**, *134*, 644–656. [CrossRef]
8. Adeola, F.O.; Picou, J.S. Social Capital and the Mental Health Impacts of Hurricane Katrina: Assessing Long-Term Patterns of Psychosocial Distress. *Int. J. Mass Emerg. Disasters.* **2014**, *32*, 121–156.
9. Yang, W.; Yin, B.; Feng, X.; Yang, D.; Gao, G.; Chen, H. The Effect of Nonlinear Factors on Tide-Surge Interaction: A Case Study of Typhoon Rammasun in Tieshan Bay, China. *Estuar. Coast. Shelf Sci.* **2019**, *219*, 420–428. [CrossRef]
10. Kang, K.; Kim, D. Retrieval of Sea Surface Velocity during Tropical Cycnes from RADARSAT-1 ScanSAR Doppler Centroid Measurements. In Proceedings of the 2015 IEEE 5th Asia-Pacific Conference on Synthetic Aperture Radar (APSAR), Singapore, 1–4 September 2015; pp. 610–613. [CrossRef]
11. Mo, D.; Hou, Y.; Li, J.; Liu, Y. Study on the storm surges induced by cold waves in the Northern East China Sea. *J. Mar. Sys.* **2016**, *160*, 26–39. [CrossRef]
12. Maloney, E.; Hartmann, D. Modulation of Hurricane activity in the Gulf of Mexico by the Madden-Julian Oscillation. *Science* **2000**, *287*, 2002–2004. [CrossRef]
13. Maloney, E.D.; Hartmann, D.L. Modulation of Eastern North Pacific Hurricanes by the Madden-Julian Oscillation. *J. Climate* **2000**, *13*, 1451–1460. [CrossRef]

14. Schenkel, B.A.; Hart, R.E. An Examination of Tropical Cyclone Position, Intensity, and Intensity Life Cycle within Atmospheric Reanalysis Datasets. *J. Climate* **2012**, *25*, 3453–3475. [CrossRef]
15. Thorne, P.W.; Vose, R.S. Reanalyses Suitable for Characterizing Long-Term Trends. *Bull. Am. Meteorol. Soc.* **2010**, *91*, 353–361. [CrossRef]
16. Saha, S.; Moorthi, S.; Wu, X.; Wang, J.; Nadiga, S.; Tripp, P.; Behringer, D.; Hou, Y.T.; Chuang, H.Y.; Iredell, M.; et al. The NCEP Climate Forecast System Version 2. *J. Climate* **2012**, *27*, 2185–2208. [CrossRef]
17. Hersbach, H.; Bell, B.; Berrisford, P.; Hirahara, S.; Horányi, A.; Muñoz-Sabater, J.; Nicolas, J.; Peubey, C.; Radu, R.; Schepers, D.; et al. The ERA5 Global Reanalysis. *Q. J. R. Meteorolog. Soc.* **2020**, *146*, 1999–2049. [CrossRef]
18. Gelaro, R.; Mccarty, W.; Suárez, M.; Todling, R.; Zhao, B. The Modern-Era Retrospective Analysis for Research and Applications, Version 2 (MERRA-2). *J. Climate* **2017**, *30*, 5419–5454. [CrossRef]
19. Kazutoshi, O.; Kamahori, H.; Ota, Y.; Takahashi, K.; Harada, Y. The JRA-55 Reanalysis: General Specifications and Basic Characteristics. *J. Meteorol. Soc. Jpn.* **2015**, *93*, 5–48. [CrossRef]
20. Liu, Z.Q.; Shi, C.X.; Zhou, Z.J. CMA Global Reanalysis (CRA-40): Status and Plans. *In Proceedings of the International Conference on Reanalysis,* Rome, Italy, 13–17 September 2017.
21. Jourdain, N.C.; Barnier, B.; Ferry, N.; Vialard, J.; Menkes, C.E.; Lengaigne, M.; Parent, L. Tropical Cyclones in Two Atmospheric (Re)Analyses and Their Response in Two Oceanic Reanalyses. *Ocean Model.* **2014**, *73*, 108–122. [CrossRef]
22. Scardino, G.; Scicchitano, G.; Chirivì, M.; Costa, P.J.M.; Luparelli, A.; Mastronuzzi, G. Convolutional Neural Network and Optical Flow for the Assessment of Wave and Tide Parameters from Video Analysis (LEUCOTEA): An Innovative Tool for Coastal Monitoring. *Remote Sens.* **2022**, *14*, 2994. [CrossRef]
23. Hatsushika, H.; Tsutsui, J.; Onogi, K.; Fiorino, M. Impact of Wind Profile Retrievals on the Analysis of Tropical Cyclones in the JRA-25 Reanalysis. *J. Meteorol. Soc. Jpn.* **2006**, *84*, 891–905. [CrossRef]
24. Kazutoshi, O.; Junichi, T.; Hiroshi, K.; Masami, S.; Shinya, K.; Hiroaki, H.; Takanori, M.; Nobuo, Y.; Hirotaka, K.; Kiyotoshi, T. The JRA-25 Reanalysis. *J. Meteorol. Soc. Jpn.* **2007**, *85*, 369–432. [CrossRef]
25. Roth, D.M. A Fifty Year History of Subtropical Cyclones. In Proceedings of the 5th Conference on Hurricanes and Tropical Meteorology, San Diego, CA, USA, 29 April–3 May 2002; p. 43.
26. Guishard, M.P.; Evans, J.L.; Hart, R.E. Atlantic Subtropical Storms. Part II: Climatology. *J. Climate* **2009**, *22*, 3574–3594. [CrossRef]
27. Truchelut, R.E.; Hart, R.E. Quantifying the Possible Existence of Undocumented Atlantic Warm-core Cyclones in NOAA/CIRES 20th Century Reanalysis Data. *Geophys. Res. Lett.* **2011**, *38*, L08811. [CrossRef]
28. Kim, H.; Lee, M.I.; Kim, S.; Lim, Y.K.; Schubert, S.D.; Molod, A.M. Representation of Tropical Cyclones by the Modern-Era Retrospective Analysis for Research and Applications Version 2. *Asia-Pac. J. Atmos. Sci.* **2021**, *57*, 35–49. [CrossRef]
29. Aryal, Y.; Villarini, G.; Zhang, W.; Vecchi, G. Long term changes in flooding and heavy rainfall associated with North Atlantic tropical cyclones: Roles of the North Atlantic Oscillation and El Niño-Southern Oscillation. *J. Hydrol.* **2018**, *559*, 698–710. [CrossRef]
30. Villarini, G.; Zhang, W.; Miller, P.; Johnson, D.; Grimley, L.; Roberts, H. Probabilistic rainfall generator for tropical cyclones affecting Louisiana. *Int. J. Climatol.* **2021**, *42*, 1789–1802. [CrossRef]
31. Wang, H.; Ting, M. Seasonal Cycle of the Climatological Stationary Waves in the NCEP–NCAR Reanalysis. *J. Atmospheric Sci.* **1999**, *56*, 3892–3919. [CrossRef]
32. Brooks, H.E.; Anderson, A.R.; Riemann, K.; Ebbers, I.; Flachs, H. Climatological Aspects of Convective Parameters from the NCAR/NCEP Reanalysis. *Atmos. Res.* **2007**, *83*, 294–305. [CrossRef]
33. Decker, M.; Brunke, M.A.; Wang, Z.; Sakaguchi, K.; Zeng, X.; Bosilovich, M.G. Evaluation of the Reanalysis Products from GSFC, NCEP, and ECMWF Using Flux Tower Observations. *J. Climate* **2010**, *25*, 1916–1944. [CrossRef]
34. Moalafhi, D.B.; Evans, J.P.; Sharma, A. Evaluating Global Reanalysis Datasets for Provision of Boundary Conditions in Regional Climate Modelling. *Clim. Dyn.* **2016**, *47*, 2727–2745. [CrossRef]
35. Vishnu, S.; Sanjay, J.; Krishnan, R. Assessment of Climatological Tropical Cyclone Activity Over the North Indian Ocean in the Cordex-south Asia Regional Climate Models. *Clim. Dyn.* **2019**, *53*, 5101–5118. [CrossRef]
36. Bengtsson, L.; Hodges, K.I.; Esch, M. Tropical Cyclones in A T159 Resolution Global Climate Model: Comparison with Observations and Re-Analyses. *Tellus* **2007**, *59*, 396–416. [CrossRef]
37. Karl, H.; Chalonge, L.; Reghezza, M.; Augendre, M. The Reanalysis of the Tropical Cyclones Intensity in the South Pacific during the 1982–1983 El Nino. In Proceedings of the 28th Conference on Hurricanes and Tropical Meteorology, Orlando, FL, USA, 28 April–2 May 2008.
38. Larow, T. An Analysis of Tropical Cyclones Impacting the Southeast United States from a Regional Reanalysis. *Reg. Environ. Chang.* **2013**, *13*, S35–S43. [CrossRef]
39. Ridder, N.; Vries, H.D.; Drijfhout, S.; Henk, V.; Meijgaard, E.V.; Vries, H.D. Extreme Storm Surge Modelling in the North Sea. *Ocean Dyn.* **2018**, *68*, 255–272. [CrossRef]
40. Dullaart, J.; Muis, S.; Bloemendaal, N.; Aerts, J. Advancing Global Storm Surge Modelling Using the New ERA5 Climate Reanalysis. *Clim. Dyn.* **2020**, *54*, 1007–1021. [CrossRef]
41. Glahn, B.; Taylor, A.; Kurkowski, N.; Shaffer, W.A. The Role of the SLOSH Model in National Weather Service Storm Surge Forecasting. *Natl. Wea. Dig.* **2009**, *33*, 3–14.

42. Greenslade, G.D.; Taylor, A.; Freeman, J.; Sims, H.; Schulz, E.; Colberg, F.; Divakaran, P.; Velic, M.; Kepert, J. *A First Generation Dynamical Tropical Cyclone Storm Surge Forecast System Part 1: Hydrodynamic Model*; Resreport, Bureau Research Reports; Australian Bureau of Meteorology: Melbourne, Australian, 2018.

43. Holland, G.J. An Analytic Model of the Wind and Pressure Profiles in Hurricanes. *Mon. Weather Rev.* **1980**, *108*, 1212–1218. [CrossRef]

44. Gao, J.; Luettich, R.; Fleming, J. Development Andinitial Evaluation of a Generalized Asymmetric Tropical Cyclonevortex Model in ADCIRC. In Proceedings of the ADCIRC Users Group Meeting, Ortley Beach, NJ, USA, 29–30 April 2013; Volume 16.

45. Willoughby, H.E.; Rahn, M.E. Parametric Representation of the Primary Hurricane Vortex. Part I: Observations and Evaluation of the Holland (1980) Model. *Mon. Weather Rev.* **2004**, *134*, 1102–1120. [CrossRef]

46. Ueno, T. Numerical Computations of the Storm Surges in Tosa Bay. *J. Oceanogr. Soc. Jpn.* **1981**, *37*, 61–73. [CrossRef]

47. Powell, M.D.; Houston, S.H.; Amat, L.R.; MorisseauLeroy, N. The HRD Real-time Hurricane Wind Analysis System. *J. Wind Eng. Ind. Aerodyn.* **1998**, *77–78*, 53–64. [CrossRef]

48. Bricheno, L.M.; Soret, A.; Wolf, J.; Jorba, O.; Baldasano, J.M. Effect of High-Resolution Meteorological Forcing on Nearshore Wave and Current Model Performance. *J. Atmos. Ocean Tech.* **2013**, *30*, 1021–1037. [CrossRef]

49. Li, X.; Han, G.; Yang, J.; Chen, D.; Zheng, G.; Chen, N. Using Satellite Altimetry to Calibrate the Simulation of Typhoon Seth Storm Surge off Southeast China. *Remote Sens.* **2018**, *10*, 657. [CrossRef]

50. Li, X.; Yang, D.; Han, G.; Yang, L.; Wang, J.; Yang, J.; Chen, D.; Zheng, G. Exploiting the Potential of Coastal GNSS-R for Improving Storm Surge Modeling. *IEEE Geosci. Remote. Sens. Lett.* **2021**, *18*, 1134–1138. [CrossRef]

51. Knapp, K.R.; Kruk, M.C.; Levinson, D.H.; Diamond, H.J.; Neumann, C.J. The International Best Track Archive for Climate Stewardship (IBTrACS). *Bull. Am. Meteorol. Soc.* **2010**, *91*, 363–376. [CrossRef]

52. Knapp, K.; Diamond, H.; Kossin, J.; Kruk, M.; Schreck, C. *International Best Track Archive for Climate Stewardship (IBTrACS) Project, Version 4*; NOAA National Centers for Environmental Information: Boulder, CO, USA, 2018. [CrossRef]

53. Uhlhorn, E.W.; Black, P.G.; Franklin, J.L.; Goodberlet, M.; Carswell, J.; Goldstein, A.S. Hurricane Surface Wind Measurements from an Operational Stepped Frequency Microwave Radiometer. *Mon. Weather Rev.* **2007**, *135*, 3070–3085. [CrossRef]

54. Gao, Y.; Sun, J.; Zhang, J.; Guan, C. Extreme Wind Speeds Retrieval Using Sentinel-1 IW Mode SAR Data. *Remote Sens.* **2021**, *13*, 1867. [CrossRef]

55. Swift, C.; DeHority, D.; Black, P.G.; Chien, J.Z. Microwaveremotesensing of Ocean Surface Wind Speedand Rain Ratesover Tropical Storms. In Proceedings of the URSI Commission F Symposium and Workshop; Frontiers of Remote Sensing of the Oceans and Troposphere from Air and Space Platforms: Shoresh, Israel, 1984; pp. 281–286.

56. Klotz, B.W.; Uhlhorn, E.W. Improved Stepped Frequency Microwave Radiometer Tropical Cyclone Surface Winds in Heavy Precipitation. *J. Atmos. Ocean Tech.* **2014**, *31*, 2392–2408. [CrossRef]

57. Said, F.; Long, D. Effectiveness Of QuikSCAT's Ultra-High Resolution Images in Determining Tropical Cyclone Eye Location. In Proceedings of the 2008 IEEE International Geoscience and Remote Sensing Symposium, Boston, MA, USA, 8–11 July 2008. [CrossRef]

58. Irish, J.L.; Resio, D.T.; Ratcliff, J.J. The Influence of Storm Size on Hurricane Surge. *J. Phys. Oceanogr.* **2008**, *38*, 2003–2013. [CrossRef]

59. Meissner, T.F.; Ricciardulli, L. *Ocean Vector Winds in Storms from the SMAP L-Band Radiometer*; Technical Report; International Meeting of Measuring High Wind Speeds Over the Ocean: Exeter, UK, 2016.

60. Ricciardulli, L.; Mears, C.; Manaster, A.; Meissner, T. Assessment of CYGNSS Wind Speed Retrievals in Tropical Cyclones. *Remote Sens.* **2021**, *13*, 5110. [CrossRef]

61. Manaster, A.; Ricciardulli, L.; Meissner, T. Tropical Cyclone Winds from WindSat, AMSR2, and SMAP: Comparison with the HWRF Model. *Remote Sens.* **2021**, *13*, 2347. [CrossRef]

62. Zehnder, J.A. The Influence of Large-scale Topography on Barotropic Vortex Motion. *J. Atmos. Sci.* **1993**, *50*, 2519–2532. [CrossRef]

63. Portmann, R.; González-Alemán, J.; Sprenger, M.; Wernli, H. How an uncertain short-wave perturbation on the North Atlantic wave guide affects the forecast of an intense Mediterranean cyclone (Medicane Zorbas). *Weather. Clim. Dyn.* **2020**, *1*, 597–615. [CrossRef]

64. Scicchitano, G.; Scardino, G.; Monaco, C.; Piscitelli, A.; Milella, M.; De Giosa, F.; Mastronuzzi, G. Comparing Impact Effects of Common Storms and Medicanes along the Coast of South-eastern Sicily. *Mar. Geol.* **2021**, *439*, 106556. [CrossRef]